ECS Solid State Letters, **3** (8) M33-M36 (2014)
2162-8742/2014/3(8)/M33/4/$31.00 © The Electrochemical Society

Nitrogen-Doped TiO_2 Nanoparticle-Carbon Nanofiber Composites as a Counter Electrode for Pt-Free Dye-Sensitized Solar Cells

Ha-Rim An,[a] HyeLan An,[a] Woo-Byoung Kim,[b] and Hyo-Jin Ahn[a,z]

[a]*Department of Materials Science and Engineering, Seoul National University of Science and Technology, Seoul 139-743, Korea*
[b]*Department of Energy Engineering, Dankook University, Cheonan-si 330-714, Korea*

Nitrogen-doped TiO_2 nanoparticle-carbon nanofiber (CNF) composites were synthesized using one-pot electrospinning. As the amount of nitrogen-doped TiO_2 nanoparticles in the composites was increased from 3.4 to 13.8 wt%, the electrochemical and photovoltaic properties in dye-sensitized solar cells (DSSCs) were evaluated. DSSCs fabricated with composites containing 13.8 wt% nitrogen-doped TiO_2 nanoparticles showed the highest current density (15.65 mA/cm^2), highest fill factor (60.50%), and superb power-conversion efficiency (6.31%). These improved properties are the result of the rough surfaces of the CNFs that serve as sites for reduction of I_3^- ions and the existence of TiN phases in the composites that reduced charge transfer resistance.
 [DOI: 10.1149/2.0061408ssl]

Manuscript submitted April 30, 2014; revised manuscript received June 3, 2014. Published June 11, 2014.

Dye-sensitized solar cells (DSSCs) have been actively studied since 1991 owing to their advantages such as a simple structure, low fabrication costs, environmental friendliness, and promising light harvesting efficiency.[1] DSSCs are commonly composed of three main components: a working electrode, a counter electrode, and an electrolyte. In this study, a porous nanocrystalline TiO_2 electrode was use for the working electrode. This type of electrode was because it exhibits the highest power-conversion efficiency compared to other semiconductors (ZnO, Nb_2O_5, In_2O_3, and SnO_2) because of large surface area for dye adsorption and ~0.2 eV lower conduction band edge than the lowest unoccupied orbital (LUMO) of Ru-based dyes for effective electron injection.[1–3] For the counter electrode, pure Pt is most commonly used as an essential component to decrease the overpotential and enable the reduction of I_3^- to I^- in electrolyte. It is well-known, however, that pure Pt is an expensive material that has limited availability and is subject to frequent price increases.[4,5] For these reasons, the development of Pt-free catalysts is important to achieving low-cost DSSCs.[4,6,7] Among alternative catalysts for Pt, carbon nanofibers (CNFs) have received considerable attention for use as counter electrodes because of their numerous advantages including low-cost, abundance, large surface area, and high catalytic activity with chemical stability against I^- redox reactions.[7] Despite these advantages, researchers reported that single CNFs exhibited lower conversion efficiency than pure Pt.[8] In order to improve the performance of the single CNFs, researchers reported physically mixing CNF and metal-oxide nanoparticles to create a counter electrode.[8,9] Despite this alternative approach, problems with low power conversion efficiency still remain. To address these problems, our strategy in this study was to synthesize nitrogen-doped TiO_2 nanoparticle-CNF composites containing three different amounts of nitrogen-doped TiO_2 nanoparticles and investigate their optimum photovoltaic performance for Pt-free DSSCs. In addition, we employed electrospinning, a simple and versatile technique suitable for synthesizing continuous nanofibers, to fabricate the CNFs.

Experimental

Nitrogen-doped TiO_2 nanoparticle-CNF composites were synthesized using one-pot electrospinning. First, a precursor solution containing polyacrylonitrile (PAN, M_w = 150,000 g/mol, Aldrich) and poly(vinylpyrrolidone) (PVP, M_w = 1,300,000 g/mol, Aldrich) in N, N-Dimethylformamide (DMF, Aldrich) was used to synthesize the CNFs. Then, TiO_2 nanoparticles (P25, Degussa) are dispersed in the precursor solution in order to synthesize the nitrogen-doped TiO_2 nanoparticle-CNF composites. To investigate the optimum conditions between TiO_2 nanoparticles and the CNFs, we created composites with weight ratios of TiO_2 nanoparticles (P25, Degussa) to precursor solution of 3.4, 9.6, and 13.8 wt% (referred as sample A, sample B, and sample C, respectively). For the electrospinning, the prepared solution was transferred into a plastic syringe. The voltage and feeding rate were fixed at ~13 kV and ~0.03 mL/h. The as-spun composites were calcined by two-step processes including stabilization (230 °C for 2 h in air) and carbonization (800 °C for 2 h in N_2 gas).

In this study, nitrogen-doped TiO_2 nanoparticle-CNF composites were used as the counter electrode in Pt-free DSSCs. In order to fabricate paste inks for the counter electrode, the prepared samples, ketjen black (KJB, Alfa Aesar), and polyvinylidene difluoride (PVDF, Alfa Aesar) were mixed in N-methylpyrrolidone (NMP, SAMCHUN) using an agate mortar and then the inks were ground for 4 h. Well-dispersed inks were then squeeze-printed onto fluorine-doped tin oxide glasses (FTO, 8 Ω/□, Pilkington). The printed FTO glasses were dried in an oven at 100°C for 12 h. For comparison, a Pt counter electrode was fabricated by spin-coating a sol-solution containing chloroplatinic acid hydrate ($H_2PtCl \cdot xH_2O$, Aldrich), which was annealed at 450°C for 0.5 h. For the working electrode, the paste inks containing P25, hydroxypropyl cellulose (HPC, M_w = ~80,000 g/mol, Aldrich), acetyl acetone (Aldrich), and de-ionized (DI) water were mixed and ground for 3 h. Then, the paste inks were squeeze-printed onto FTO glasses. TiO_2 nanoparticle coated FTO glasses were annealed at 500°C for 1 h before they were immersed in a dye solution consisting of N719 ($Ru(dcbpy)_2(NCS)_2$, Solaronix) in ethanol for 24 h. A 0.6 M BMII (1-Butyl-3-methylimidazolium iodide)-based iodine solution was used as an electrolyte to fill the gap between the counter and working electrodes.

The morphological properties of all samples were characterized by field-emission scanning electron microscopy (FESEM, Hitachi S-4700) and transmission electron microscopy (MULTI/TEM; Tecnai G^2, KBSI Gwangju Center), respectively. The structural and chemical properties were examined by X-ray diffraction (XRD, Rigaku X-ray diffractormeter) and X-ray photoelectron spectroscopy (XPS, ESCALAB250), respectively. The electrochemical properties of the DSSCs were evaluated using a potentiostat/galvanostat (Eco Chemie, PGST302N). The photovoltaic properties of DSSCs were measured using a solar simulator (McScience, K101 LAB20) with a light intensity of 100 mA/cm^2 using a 150 W xenon lamp.

Results and Discussion

Figure 1a-1d display FESEM images obtained from the single CNFs and samples A-C. The diameters of the samples are in the range of ~191 to 232 nm for the single CNFs, ~194 to 261 nm for sample A, ~189 to 322 nm for sample B, and ~281 to 358 nm for sample C. While the single CNFs display a smooth surface morphology, samples A-C exhibit rough and uneven CNF surfaces because of the embedment of nitrogen-doped TiO_2 nanoparticles within CNFs. As the relative weight ratio of nitrogen-doped TiO_2 nanoparticles in composites

[z]E-mail: hjahn@seoultech.ac.kr

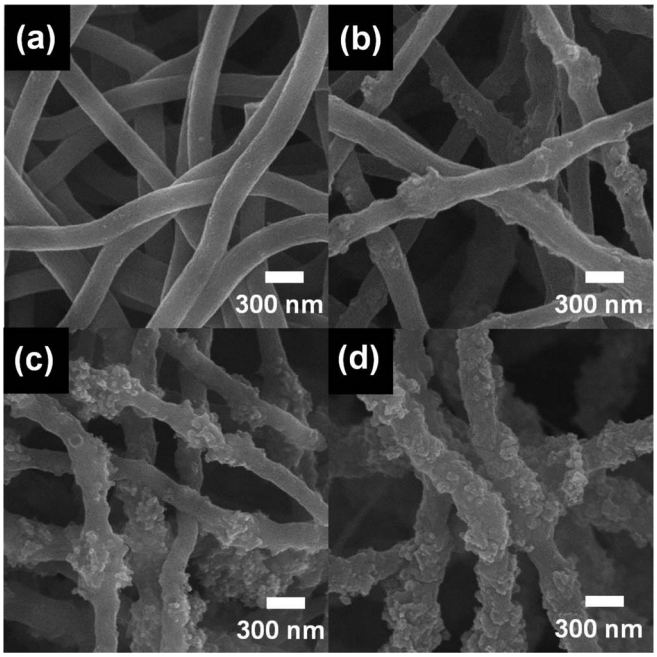

Figure 1. FESEM images of (a) single CNFs, (b) sample A, (c) sample B, and (d) sample C.

increased, the diameter and surface roughness of the composites also increased. In addition, all samples maintain the shape of nanofibers despite the embedment of nitrogen-doped TiO_2 nanoparticles.

Figure 2 displays TEM images obtained from the single CNF and sample C. The single CNF in Figure 2a exhibits wholly a bright-gray contrast in the CNF matrix, implying the existence of one phase in the nanofibers. As shown in Figure 2b, one-dimensional (1-D) composites are composed of nitrogen-doped TiO_2 nanoparticles and CNF as indicated by the presence of relatively dark-gray and bright-gray contrasts. Nitrogen-doped TiO_2 nanoparticles, which are in the range of ∼ 21 nm to ∼35 nm in diameter, are well dispersed within the CNF

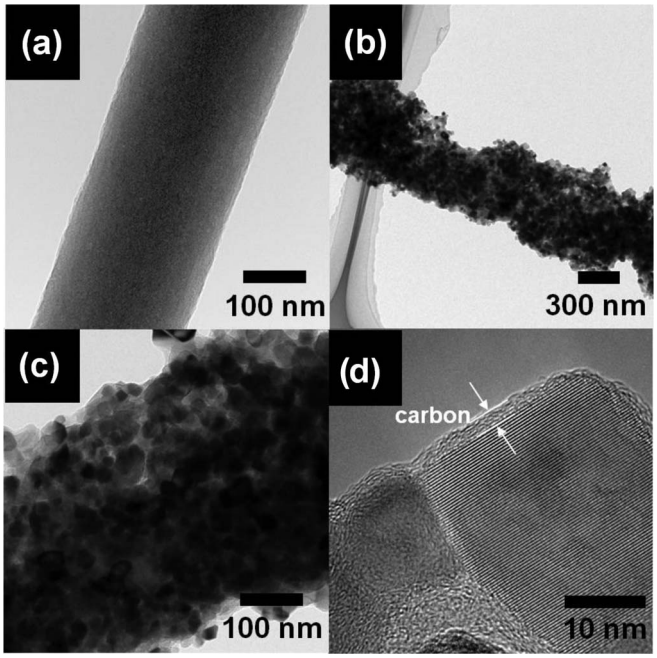

Figure 2. TEM images obtained from (a) single CNFs and (b-d) sample C.

matrix as seen in Figure 2c. The high-resolution TEM image shown in Figure 2d confirms that crystalline nitrogen-doped TiO_2 nanoparticles are surrounded by amorphous carbon materials as indicated by the relatively bright contrast. Further, this result indicates that nitrogen-doped TiO_2 nanoparticles are embedded within the CNF, implying the successful formation of nitrogen-doped TiO_2 nanoparticle-CNF composites.

Figure 3a presents XRD data from single CNFs and samples A-C. The single CNFs display broad peaks at approximately 25° and 43°, corresponding to the (002) and (100) layers of the graphite. For samples A-C, one set of characteristic peaks are observed at $2\theta = 25.5°$, 37.9°, 48.2°, 54.1°, and 62.6°, corresponding to the (101), (004), (200), (105), and (204) planes of anatase TiO_2 phases (space group $I4_1/amd$ (141), JCPDS card No. 841286). Another set of characteristic peaks is observed at $2\theta = 27.6°$, 36.3°, 41.5°, and 55.1°, corresponding to the (110), (101), (111), and (211) planes of rutile TiO_2 phases (space group p42/mnm (136), JCPDS card No. 870920). In addition, a TiN phase is observed at $2\theta = 43°$, corresponding to the (200) plane, implying that the TiN phase in composites is formed by N_2 gas during carbonization.[10] Further, TiN, which is similar to the electronic structure of the noble metal, possesses superb catalytic activity for the reduction of I_3^- ions. The structural change of TiO_2 by nitrogen doping is also demonstrated. As seen in Figure 3a, increased amounts of nitrogen-doped TiO_2 in composites result in reduced peak intensities of the rutile (110) phase while those of the anatase (101) phase are increased. It was reported that nitrogen doping causes a reconstruction of the rutile owing to N^{3-}-substituting O^{2-} lattice, resulting in formation of defects that act as hole trapping sites.[11] This result could affect the current density of DSSCs. To investigate chemical bonding states of sample C, XPS measurements were performed and the results are displayed in Figure 3b-3c. The XPS core-level spectra of the Ti $2p_{3/2}$ photoelectrons are mainly observed at ∼459.0 eV (TiO_2), ∼458.7 eV (N-TiO_2), and ∼456.0 eV (TiN), while the core-level spectra of the Ti $2p_{1/2}$ photoelectrons are observed at ∼465.1 eV (TiO_2), ∼463.8 eV (N-TiO_2), and 461.7 eV (TiN). In particular, atomic percentages of N-TiO_2 and TiN elements in sample C are 3.7% and 2.5%, which were calculated by $C_x = (I_x/S_x)/(\Sigma I_i/S_i)$ based on the XPS spectra. Furthermore, the O 1*s* core-level is observed as a sharp peak at ∼530.2 eV (TiO_2) and a broad peak at ∼532.0 eV (N-TiO_2). Based on the XRD and XPS results, the chemical bonding states of elemental Ti consisted of TiO_2 phases, nitrogen-doped TiO_2 phases, and TiN phases.

Figure 4a displays the cyclic voltammetry (CV) curves of pure Pt, single CNF, and samples A-C in I_3^-/I^- system at a scan rate of 50 mVs^{-1} from −0.3 to 1.1 V. The catalytic performance of the prepared samples was compared with Pt, which is known as an excellent catalyst. To facilitate reaction between the counter electrode and the electrolyte, electrons are injected into oxidized dye from I^- ions in the electrolyte, and the produced I_3^- ions are reduced at the counter electrode. CV curves shown in Figure 4a indicate that two pairs of redox reactions are observed. Specifically, the positive and negative pairs correspond to the oxidation reaction of I_2/I_3^- and the reduction reaction of I_3^-/I^-, respectively.[12] In particular, when the reaction of $I_3^- + 2e^- \rightarrow 3I^-$ is considered, sample C exhibited the highest redox current density amongst all samples. As obtained from the CV curves, oxidation peaks of pure Pt, single CNF, sample A, sample B, and sample C are 1.19, 1.51, 2.01, 2.83, and 3.06 mA/cm^2, respectively, at 0.51 V. The reduction peaks of pure Pt, single CNF, sample A, sample B, and sample C are −1.35, −1.94, −2.49, −3.36, and −3.85 mA/cm^2, respectively, at −0.22 V. Compared to the other samples, sample C exhibited a superb current density that is attributable to the high CNF surface roughness that serve as sites for the enhanced reduction of I_3^- ions and the existence of TiN phases within the composites for high catalytic activity. This result leads to an increase in the redox reaction rate occurring at the counter electrode and enhances catalytic activity for the counter electrode in Pt-free DSSCs.

Figure 4b displays the photocurrent density(J)-voltage(V) curves of DSSCs fabricated with the prepared counter electrodes. The photovoltaic parameters of all samples are listed in Table I. Single CNFs exhibited the lowest photocurrent density (J_{sc}, 12.59 mA/cm^2) and

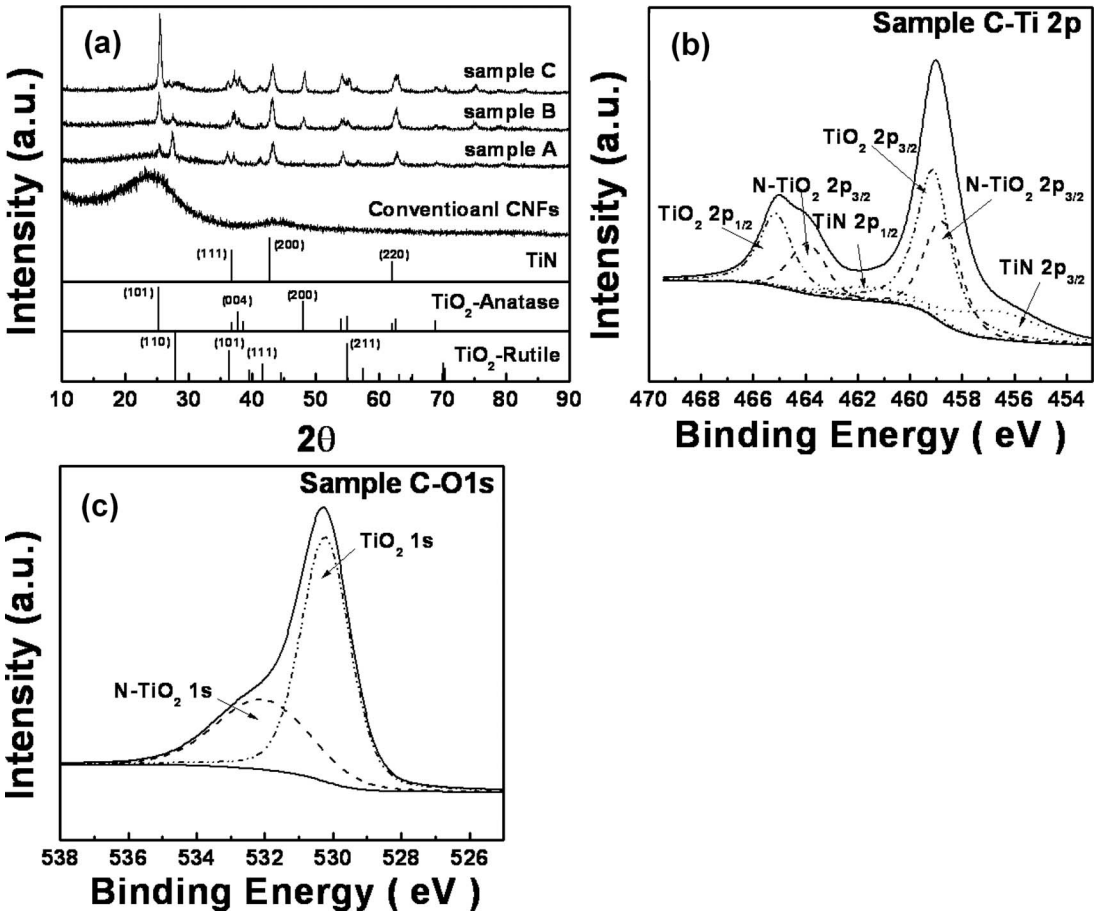

Figure 3. (a) XRD data obtained from single CNFs and samples A-C. XPS core-level spectra of (b) Ti 2*p* and (c) O 1*s* obtained from sample C.

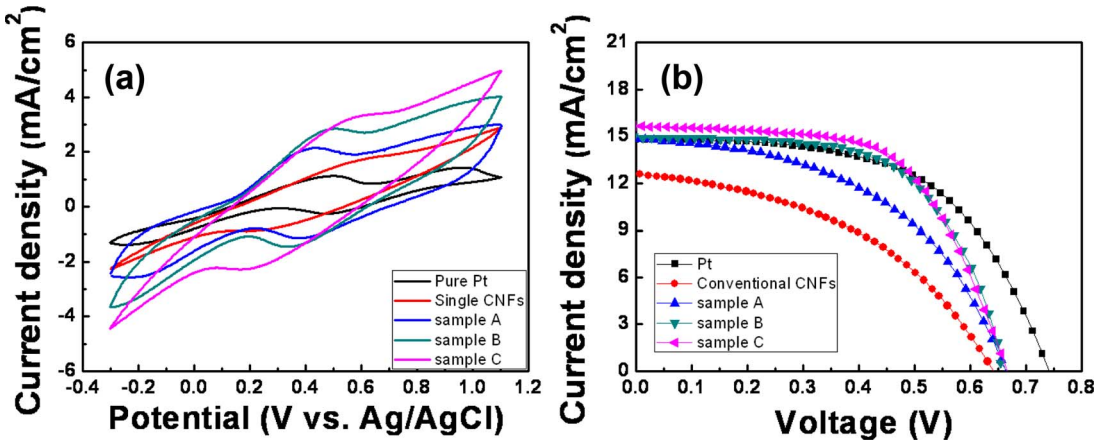

Figure 4. (a) CV curves of pure Pt, single CNFs, sample A, sample B, and sample C measured at a scan rate of 50 mVs^{-1} from −0.3 to 1.1 V. (b) Photocurrent density-voltage characteristics of DSSCs fabricated with pure Pt, single CNFs, sample A, sample B, and sample C.

Table I. Photovoltaic parameters of DSSCs fabricated with pure Pt, single CNFs, sample A, sample B, and sample C.

Samples	Open circuit voltage (V_{oc}, V)	Photocurrent density (J_{sc}, mA/cm^2)	Fill factor (*ff*,%)	Power conversion effeiciency (PCE,%)
Pt	0.74	14.80 ± 0.2	57.13 ± 0.2	6.27 ± 0.1
Single CNFs	0.63	12.59 ± 0.1	43.82 ± 0.1	3.54 ± 0.1
Sample A	0.66	14.82 ± 0.2	48.96 ± 0.2	4.89 ± 0.2
Sample B	0.67	14.96 ± 0.1	59.78 ± 0.1	6.05 ± 0.1
Sample C	0.67	15.65 ± 0.2	60.50 ± 0.3	6.31 ± 0.1

fill factor (*ff*, 43.82%) values because of poor catalytic properties. As shown in Figure 4b and Table I, the open-circuit voltage (V_{oc}) for samples A-C are of similar value at ∼0.67 V, while different values of the *ff* and J_{sc} would intensively affected by the catalytic behavior of the samples. Specifically, as the amount of nitrogen-doped TiO_2 nanoparticles in composites increased, photovoltaic parameters of the samples, such as J_{sc} and *ff*, of the samples are enhanced. Therefore, the power-conversion efficiency (PCE, η) for the samples can be calculated as follows:[13]

$$\eta(\%) = [J_{sc} \times V_{oc} \times ff]/[I_{max} \times V_{max}] \quad [1]$$

where J_{sc} is the short-circuit photocurrent density, V_{oc} is the open-circuit voltage, *ff* is the fill factor, I_{max} is a maximum value of the power current, and V_{max} is a maximum value of the power voltage. The power-conversion efficiency is 3.54% for single CNFs, 4.89% for sample A, 6.05% for sample B, and 6.31% for sample C. Therefore, sample C demonstrates superior power-conversion efficiency based on having a high V_{oc} (0.67 V), the highest J_{sc} (15.65 mA/cm^2), and the highest *ff* (60.50%). The performance improvement may be attributable to the enhanced reduction of I_3^- ions because of the high surface roughness of the CNFs and the decreased charge transfer resistance resulting from the existence of TiN phases within the composite. Further, because the photovoltaic performance of sample C is slightly higher that of pure Pt, 6.31% as compared to 6.27%, TiO_2 nanoparticle-CNF composites should be considered promising candidates for use as the counter electrode in Pt-free DSSCs.

Conclusions

Nitrogen-doped TiO_2 nanoparticle-CNF composites were synthesized using electrospinning. The relative amounts of nitrogen-doped TiO_2 nanoparticles in composites were modulated and the photovoltaic properties of all samples were established. In particular, sample C, fabricated with 13.8 wt% nitrogen-doped TiO_2 nanoparticles, displayed the best catalytic properties for the counter electrode. Catalytic properties, strongly influence photovoltaic performance within DSSCs, therefore, sample C also exhibited the highest photocurrent density (15.65 mA/cm^2), the highest fill factor (60.50%), and superior power-conversion efficiency (6.31%).

Acknowledgment

This work was supported by grant No. 10046672 from the Ministry of Knowledge Economy (MKE) and R&D Program for Technology of Specialized Materials particularly designed for venture business funded by the Ministry of Knowledge Economy, Republic of Korea.

References

1. W. Maiaugree, S. Pimanpang, M. Towannang, S. Saekow, W. Jarernboon, and V. Amornkitbarmarung, *J. Non-Cryst. Solids*, **358**, 2489 (2012).
2. M.-J. Jeng, Y.-L. Wung, L.-B. Chang, and L. Chow, *Int. J. Photoenergy.*, **2013**, 8 (2013).
3. K. Hara, T. Sato, R. Katoh, A. Furube, Y. Ohga, A. Shinpo, S. Suga, K. Sayama, H. Sugihara, and H. Arakawa, *J. Phys. Chem. B*, **107**, 597 (2003).
4. J.-Y. Lin, J. -H. Liao, and T.-C. Wei, *Electrochem. Solid-State Lett.*, **14**, D41 (2011).
5. J.-L. Lan, Y.-Y. Wang, C.-C Wan, T.-C. Wei, H.-P. Feng, C. Peng, H.-P. Cheng, Y.-H. Chang, and W.-C. Hsu, *Curr. Appl. Phys.*, **10**, S168 (2010).
6. S. Yun, L. Wang, W. Guo, and T. Ma, *Electrochem. Commum.*, **24**, 69 (2012).
7. J. Lim, S. Y. Ryu, J. Kim, and Y. Jun, *Nanoscale Res. Lett.*, **8**, 227 (2013).
8. Q. Qiao, *Solar cells-Dye-Sensitized Devices*, **20**, 457 (2011).
9. P. Joshi, Y. Xie, M. Ropp, D. Galipeau, S. Bailey, and Q. Qiao, *Energy Environ. Sci.*, **2**, 426 (2009).
10. R. Trejo-Tzab, J. J. Alvarado-Gil, P. Quintana, and P. Bartolo-Perez, *Catal. Today.*, **193**, 179 (2012).
11. M. Batzill, E. H. Marales, and U. Diebold, *Phys. Rev. Lett.*, **96**, 026103 (2006).
12. S. Ameen, M. S. Akhtar, Y. S. Kim, O.-B. Yang, and H.-S. Shin, *J. Phys. Chem. C*, **114**, 4760 (2010).
13. M. Grätzel, *J. Photochem. Photobiol. C*, **4**, 145 (2003).